Mechanical Strain Tailoring via Magnetic Field Assisted 3D Printing of Iron Particles Embedded Polymer Nanocomposites

Pantea Afshari[1], Maryna Pavlyuk[1], Cristian Lira[2,*] Kali-Babu Katnam[3], Mahdi Bodaghi[4] and Hamed Yazdani Nezhad[1,5,*]

[1]Advanced Composites Research Focused Group, School of Science and Technology, City, University of London, London, UK

[2]Engineering Development, National Composites Centre, Bristol, UK

[3]Department of Mechanical, Aerospace and Civil Engineering, University of Manchester, Manchester, UK

[4]Department of Engineering, School of Science and Technology, Nottingham Trent University, Nottingham, UK

[5]School of Mechanical Engineering, Faculty of Engineering and Physical Sciences, University of Leeds, Leeds, UK

*Corresponding authors: cristian.lira@nccuk.com and h.yazdaninejad@gmail.com

Abstract

The development of efficient, energy saving, eco-friendly and automated manufacturing of free-form variable-thickness polymer composite components has created a step-change and enabling technology for the composites industry seeking geometry tailoring during a mould-less and/or additive manufacturing such as that in 3D printing. The current article presents ongoing research on the 3D printing of polymer nanocomposites embedded with ferromagnetic iron particles. This research involves exposing the nanocomposite to a magnetic field remotely during the fabrication process. The magnetic field is applied unidirectionally by using constant-strength magnets placed on a fused deposition method (FDM) based 3D printing platform. The magnets are symmetrically fixed on both sides of the printed nanocomposite. A high-performance polylactic acid (PLA) grade polymer was selected, which is commonly used for rigid structures. The setup utilised Neodymium magnets with a constant strength below 1T. The printing process maintained a consistent temperature of 220°C for the nozzle and 40°C for the bed. Observations have shown that the nanocomposites being printed undergo permanent macro-scale deformations caused by the extrinsic strains induced by the surrounding iron particles in response to the relatively low magnetic field (<1T). To provide a theoretical understanding of these induced strains, a Multiphysics constitutive equation has been developed. This equation aims to describe the micromechanics of the field-induced strains and study the evolution of magnetisation within a relatively thick nanocomposite (5mm thickness). Experimental measurements have quantified the macro-scale geometric variations achieved during printing, and a correlation has been established between these variations and the extrinsic strains derived from the theoretical solution, i.e. induced 1.3 mm. The theoretical solution accurately provides the description of the actual field induced strains during the 3D printing process provided that precise temperature values for the layers are accounted for. The theory also predicts a high sensitivity of field induced deformation to such temperatures and interconnects the Multiphysics parameters in explicit expressions for the phenomenon occurring. The results demonstrate a viable and disruptive magnetic field equipped fabrication approach with ability to extend to geometry control during its process.

Keywords: 3D printing, magnetic polarisation, polymer nanocomposite, ferromagnetic particles, composite manufacturing

1. Introduction

The advancement of efficient, energy-saving, environmentally friendly, and automated manufacturing of free-form, variable-thickness polymer composite components has brought about a significant breakthrough and empowering technology for the composites industry. This technology allows for customised shaping of geometries during the process of mould-less and/or additive manufacturing, as seen in 3D printing [1-3] and automated tow placement (ATP) [4, 5]. Moreover, aiming for sustainable manufacturing including 3D printing requires an thorough understanding and quantification of the existing state-of-the-arts in order to suggest modifications for achieving optimal cost, energy consumption and quality. As addressed in [6], design for a viable sustainable 3D printing technology such as fused filament fabrication must also account for CO2 emission and flexibility. Moreover multi-material plastic wastes and functional materials are ideal candidate to promote sustainability even further beyond the *status quo* for remanufacturing and reuse in multifunctional composites [1, 7-9]. Despite having several advantages, such as improved design flexibility, reduced production time, and lower costs, there are significant challenges associated with achieving the desired geometric features in mould-less composite manufacturing. These challenges primarily arise from the manipulation of process parameters. They include issues related to surface finish, the material's deformation caused by its viscoelastic response to manufacturing parameters, ensuring structural integrity during the laying-up process (such as 3D printing), and maintaining quality control. The absence of a mould poses difficulties in attaining consistent shape and size for the final product. On the other hand, the implementation of remote energy fields (electromagnetic and magnetic) has been introduced to tune polarisation in field-responsive materials. These materials can be either dielectric/ferroelectric or magnetic/diamagnetic or a combination. The induced polarisation energy can then be converted into strain energy, allowing for micromechanical tuning [10-15].

With sophisticated and controlled tuning, as well as a well-established correlation analysis of field deformation, remote field exposure can emerge as a promising option for free-form fabrication of multi-material systems, such as magnetic nanocomposites. For instance, electromagnetic fields (e.g., microwaves) have already been commercialised for manufacturing polymer composites at various scales [16]. However, they come with significant health and safety considerations and may interfere with the quality of electrically conductive systems such as carbon fibres due to arcing. On the other hand, magnetic fields are easier to control, and within a wide range of strengths, they do not cause arcing in systems containing conductive materials. However, their variation may generate an electromotive force that initiates an electron chain reaction, resulting in induced electric currents. Both fields face limitations in terms of penetrating materials deeply, restricting these technologies to surface-based processing in relatively thick and large structures. To overcome this, a responsive material such as ferroelectric or magnetic would be necessary for the processing.

The present article reports on a disruptive approach that aims to introduce magnetic field-assisted additive manufacturing. This method involves incorporating controllable geometric features into a fused deposition modeling (FDM) 3D printing process. The goal is to evaluate the use of relatively low magnetic fields (<1T) in inducing unidirectional deformation during the fabrication of iron particle-embedded polymer nanocomposites with a basic geometry. Apart from FDM, material extrusion, material jetting, and vat photopolymerisation are also commonly employed methods for 3D printing magneto-active composites, regardless of whether the fillers are *hard* magnets or not. It is important to note that these printing processes can be further divided into various subcategories. In the conducted research, permanent magnets were arranged in a single row and directionally aligned to create a magnetic field of equal strength on all sides. This is distinct from the Halbach Array arrangement, where the magnetic fields accumulate to nullify the resultant field away from the arrangement (See Figure 1).

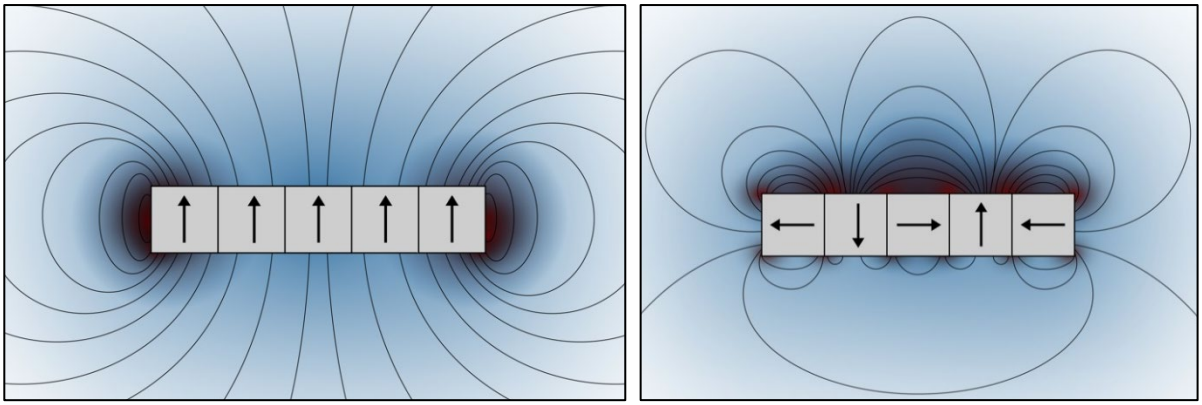

Figure 1: Single row magnet on the left and Halbach array on the right

In the present study, filaments containing iron particles were utilised for FDM printing. Iron is renowned for its ferromagnetism, which characterises materials displaying permanent magnetisation and the potential for continuous magnetic moment, even in the absence of an external field. Each iron atom consists of four unpaired electrons, referred to as magnetsation electrons, resulting in the behaviour of each iron atom as a magnetic dipole. Figure 2a illustrates individual polygons representing distinct domains exhibiting magnetic dipole characteristics. Unlike atomic distances, domains significantly exceed in size, ranging from 1 to 100 microns, as observed in this particular research. The iron particles contain randomly oriented domains, hence lacking net magnetisation. However, upon application of a magnetic field, the magnetic domains align themselves with the direction of the field, as depicted in Figure 2b. Ideally, iron sustains its alignment even after the removal of the magnetic field (Figure 2c) [17].

Magnetic materials find extensive use in various applications, including their incorporation in biomedical devices, such as three-dimensional origami structures. Origami involves the transformation of a flat sheet into a three-dimensional construction through predetermined folding, effectively harnessing its inherent shape-morphing potential. These structures exhibit intricate folding capabilities and a remarkable ability to regain their original shape, showcasing superior programmability and shape-morphing properties. When coupled with stimuli-responsive characteristics, these structures hold great promise in the development of functional and self-regulating systems, thereby paving the way for the creation of magneto-active soft mechanisms [18-24]. Harnessing the potential of magneto-responsive materials also presents new opportunities for the creation of intelligent biomaterials that can generate distinctive mechanical or biological signals to regulate cellular mechanobiology. Hydrogels prove to be an excellent choice for biomedical applications, including tissue engineering, as they can be employed in the three-dimensional bioprinting of cells. By serving as a medium for embedding magnetic particles, hydrogels enable reversible shape-morphing behavior. Furthermore, the utilisation of magnetic particles in conjunction with magnetic actuation introduces novel possibilities for the remote control of cellular activity.

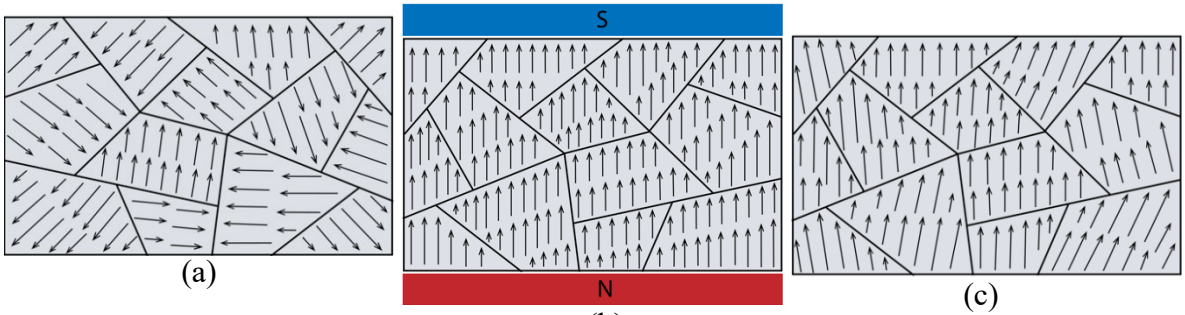

(a) (b) (c)

Figure 2. a) Domains in the iron section before the magnetic field was applied, b) Domains in the iron section while the magnetic field is applied, and c) Domains in the iron section after the magnetic field was removed

The current article attempts to answer the research questions that whether it is viable to utilise remote magnetic fields to tailor geometric features during a magnetic polymer manufacturing process such as 3D printing, and is the response of the material under process parameters (herein temperature and speed) is sufficiently sensitive to low magnetic fields for the viability purpose. To do so, a novel magnetic equipped 3D printing rig has been designed and setup to apply static magnetic field's force line on the magnetic layers being printed (section 2). Theoretical constitutive expressions have been developed (section 3) for underpinning the magnetisation of magnetic particle embedded polymer during FDM based 3D printing, when subjected to remote magnetic fields. A novel constitutive equation has been derived to interconnect such micromechanical Multiphysics phenomenon (i.e., strain energy to magnetic polarisation). Furthermore, The geometric changes induced by the magnetic field during the process have been evaluated and compared with the theoretical calculations (sections 4 and 5). The knowledge developed in this research for realisation and quantification of in-situ geometry and strain energy introduction via magnetic fields would provide geometric tailoring remotely and mould-lessly.

2. Experimental Approach

The magnetic filament materials utilised in this research are iron particle-embedded PLA filament (nominal 1.75mm diameter), supplied by Amolen®. Neodymium magnets of 10mm diameter, with the magnetic field strengths of maximum 0.3T, were embedded over a thin metal sheet which was fixed to the printing bed prior to the printing process. Such sheet was used to ensure setting up the magnets at the close proximity of the nanocomposite when it was printing. The schematic of the magnetic field equipped FDM 3D printing setup is illustrated in Figure 3 where an effective space has been identified for the application of the unidirectional field. Therefore, the nanocomposite printed over the limit enforced by the height of the magnets (~3 mm) was only magnetised and exhibited deformation.

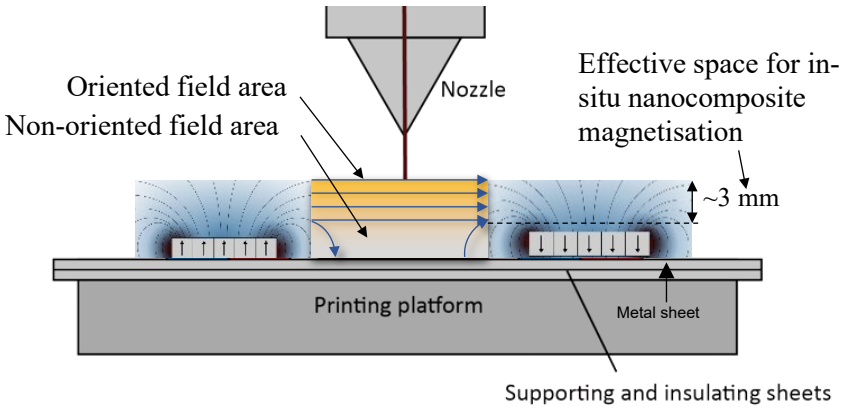

Figure 3. FDM-3D printing process with magnets embedded on either side of the printing bed, illustrating effectively oriented field and non-oriented volumes

A MakerBot Replicator 2 printer was utilised to print a basic geometry form the iron particle-embedded PLA filament, with the dimensions provided in Figure 4. Two strips of metallic plate were used to fix the magnets on the printing bed with the magnets (labelled as N and S). The final arrangement for the magnets is seen in Figure 4b, which consisted of two rows magnets on either side. The magnets were placed at the vicinity of the printing area.

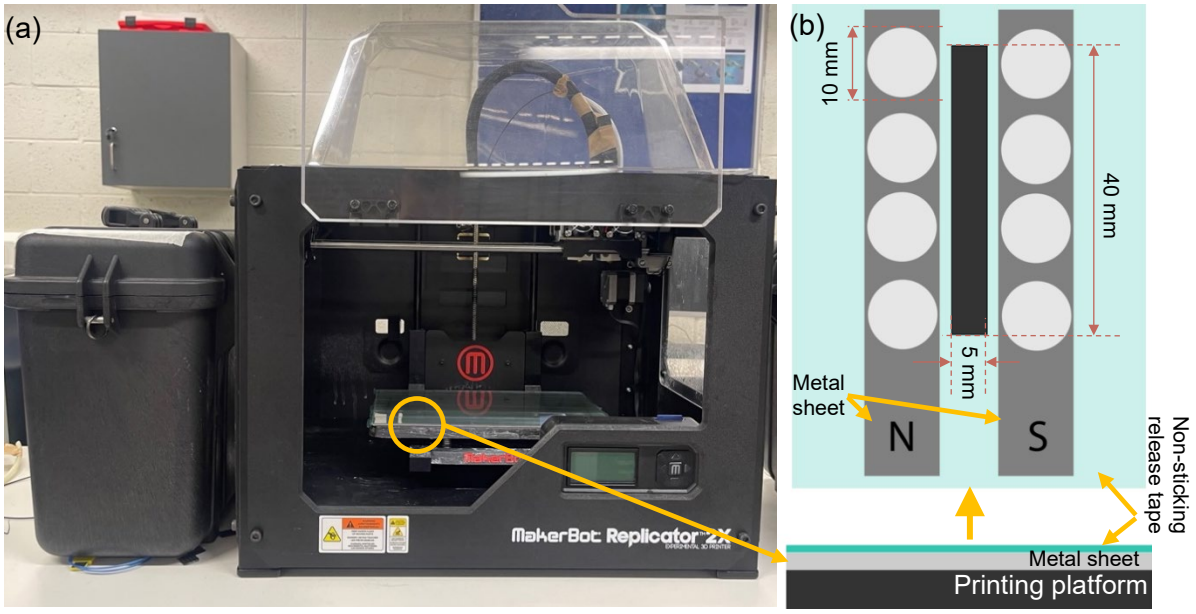

Figure 4. a) Printing set-up, b) Arrangement of the permanent magnets

The filaments had a nominal diameter of 1.75 mm and were stored in designated containers to prevent exposure to moisture or contamination. A computer-aided design (CAD) was created for a basic specimen with dimensions of 5×10×40 mm³, utilizing 100% infill for all tests. To accommodate the magnets, which were approximately 3 mm in height, around 40% of the block's height was allocated as support. This resulted in printing a 3 mm height prior to securing the magnets on the bed. Release film tape was applied to the bed to facilitate easy separation of the specimens after printing. During the experimental trial phases, various printer settings were tested to achieve high-quality printing with optimal precision. The final printer settings can be found in Table 1. Several trial stages were conducted to ensure optimal quality of the filament process, via adjusting both nozzle and platform (bed) temperatures, while maintaining the speeds. Initial examinations were conducted using higher temperatures however it was found that 220°C and 40°C provide consistent printing and minimal void creation for such filament. The printing duration for each specimen was approximately 14 minutes.

Table 1. Main printing phase parameters

Setting parameter	Value
Extruder temperature	220 °C
Platform Temperature	40 °C
Travel Speed	30 mm/s
Z – axis Travel Speed	23 mm/s
Minimum Layer Duration	5.0 s

Once each stage of the printing process was finished, the visual characteristics of each sample, such as layer separation and porosity, were thoroughly examined for quality. This qualitative analysis was carried out using a VHX Keyence Digital Microscope equipped with VH-Z20R and VH-Z500R lenses, providing magnification ranging from X20 to X200 and X500 to X5000, respectively. To assess the distribution and dispersion of iron particles throughout the specimen volume, an X-ray computed tomography scan was performed. This scanning procedure, aimed at quantifying the morphological features, took place at the Henry Royce Institute in Manchester, UK.

3. Theoretical Development of In-situ Magnetic Field Induced Deformation during 3D Printing

This section develops a theoretical constitutive equation underpinning deformation during a magnetic assisted layer-by-layer 3D printing of magnetic particles embedded polymer which is subjected to relatively low (< 1T) static magnetic fields, in-situ during the printing.

3.1. Magnetisation in ferromagnetic particle embedded polymer nanocomposite

Assuming a nanocomposite comprising micron-sized iron particles uniformly distributed in a spherical shape (with a diameter denoted as d) and embedded within a polymer matrix at a volume fraction represented by V_i in percentage, the sample, consisting of this multi-material system, is 3D-printed with a thickness indicated as t in millimeters. When subjected to an applied magnetic field denoted as B in milli-Tesla (mT), resulting from Neodymium magnets positioned with opposite poles on either side of the thickness t, the magnetic field is measured at a distance of $t/2$ from the specimen's centre. It is assumed that this measurement of the magnetic field, obtained at half the thickness of the specimen, experiences a change represented by Δ in percentage, which arises due to the divergence of the magnetic field lines. To analyze the response to an external magnetic field, the governing equation is considered as follows [25, 26]:

$$\boldsymbol{B} = \mu_0(\boldsymbol{H} + \boldsymbol{M}) \tag{1}$$

where μ_0 is the free-space magnetic permeability, $\boldsymbol{H}$ the external magnetic field, $\boldsymbol{M}$ the magnetic moment, and $\boldsymbol{B}$ the magnetic induction. Since the field inside the material is not uniform and is assumed to be reduced linearly by Δ% at a distance of z from the magnetically exposed surface, we can assume that the field follows a linear gradient:

$$H(z) = H\left(1 - \frac{2z}{t}\Delta\right) \tag{2}$$

where z is the normal distance from the exposed surface ($0 \leq z \leq t$). At $z = 0 \rightarrow H(z) = H$, and at $z = t \rightarrow H(z) = H(1 - 2\Delta/100)$.

To calculate the magnetic moment of a single iron particle, magnetic susceptibility is utilized herein:

$$M_{particle} = \chi_{particle}\, H(z) \tag{3}$$

where $\chi_{particle}$ is the magnetic susceptibility of the particle. Substituting equation (2) in (3) for a given particle at distance z from the magnetically exposed surface:

$$M(z) = \chi_{particle}\, H\left(1 - \frac{2z}{t}\Delta\right). \tag{4}$$

At $z = 0$, M describes the magnetisation at the particles at the exposed surface while with the increasing z, the magnitude of M decreases linearly with the reduction rate of Δ%. Note that the expression in Eq. (4) has been derived based on the assumption that the iron particles are uniformly distributed in the polymer matrix. In actual samples, the distribution of the particles and the magnetic field inside the material can be unevenly distributed (as also observed during optical microscopy and X-ray scanning in this research), and a more detailed model may be required to accurately describe the magnetisation of the nanocomposite material.

3.2. Theoretical derivation of micromechanics in ferromagnetic particle embedded polymer nanocomposite

In this section, firstly, a brief overview of the concept of the Eshelby tensor for isotropic materials in elasticity is presented, and then its application to the mean-field homogenization

techniques for investigating the effective properties of multi-phase composites comprising of particles embedded polymer will be discussed.
The single inclusion problem, proposed by J.D. Eshelby, is depicted in Figure 5. The inclusion is deformed by the eigenstrain of ε^* in a stress-free condition and then inserted to the hole while is subjected to the traction, T, to maintain its original shape. After releasing the traction, the inclusion expands according to a constrained strain of ε^c due to the interaction with the matrix. The constrained strain is related to the eigenstrain as used in [27]:

$$\varepsilon_{ij}^{c} = S_{ijkl}\, \varepsilon_{kl}^{*} \tag{5}$$

where S_{ijkl} is referred to as Eshelby tensor. This tensor for a spherical inclusion in an isotropic matrix can be derived as:

$$S_{ijkl} = \frac{(5\nu-1)}{15\,(1-\nu)}\,\delta_{ij}\delta_{kl} + \frac{(4-5\nu)}{15\,(1-\nu)}\,(\delta_{ik}\delta_{jl} + \delta_{il}\delta_{jk}) \tag{6}$$

where ν is the poison's ratio and δ is the Kronecker's delta.

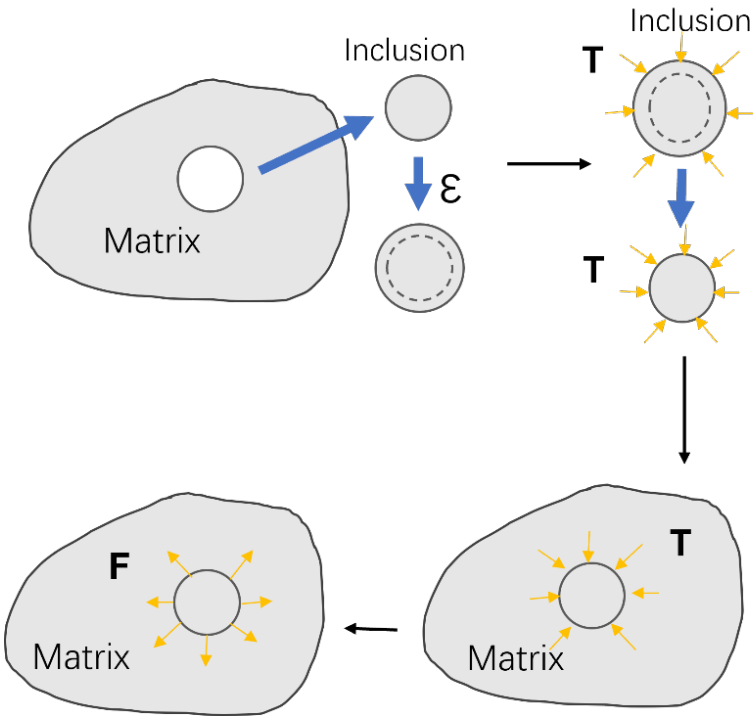

Figure 5: Single inclusion problem in elasticity [27]

While in the definition of a single inclusion problem both the inclusion and the matrix have identical elastic constants, the single inhomogeneity problem refers to an embedded inhomogeneity with a different property than the matrix, a technique so-called mean-field homogenization. For this case, the aforementioned Eshelby inclusion problem can be utilised in equivalent form to consider the difference of elastic properties between inhomogeneity and the matrix [28].
In the case of a particle-embedded polymer with multiple inhomogeneities, the Mori-Tanaka model, one of the mean-field homogenization techniques, is utilised to consider the interactions between the reinforcements. Previous studies have shown that this model can be valid for relatively low volume fractions of the inhomogeneities (< 20%), making it applicable to our specific scenario [29]. The effective elastic properties (described as tensor X_{eff}) of the nanocomposite, obtained via utilising the Mori-Tanaka model, is given by:

$$X_{eff} = \left(V_p\, X_p + V_i X_i T\right)\left(V_p I + V_i T\right)^{-1} \tag{7}$$

where X can be stiffness or compliance tensors, I is the identity tensor, V_p and V_i are the volume fractions of the polymer matrix and inhomogeneity (iron particles), respectively (i.e. $V_p + V_i = 1$), and T is given by:

$$T = \left[I + S\, X_p^{-1}\left(X_i - X_p\right)\right]^{-1} \tag{8}$$

where S is the Eshelby tensor and is calculated via Eq. (6).

3.3. Magnetic field induced localised extrinsic strains in ferromagnetic particle embedded polymer nanocomposite

To obtain an expression for localized extrinsic strain, we make the assumption that spherical functional particles (specifically iron) are uniformly and rigidly distributed within a cubic polymer matrix. One surface of the matrix is exposed to a magnetic field denoted as H. Let's assume an arbitrary particle is located at a distance z from the exposed surface. When this particle is converted into a magnetic dipole, it affects the surrounding matrix, resulting in an extrinsic strain-stress field. In reality, the mechanical and magnetic behaviours of a ferromagnetic material are interconnected, which necessitates the derivation of nonlinear constitutive equations. These equations, in turn, complicate theoretical evaluations when scaling up to account for dimensions larger than the particle size, such as that in our case. Therefore, numerical analysis becomes necessary. To simplify this nonlinear problem, our research proposes an innovative and effective theoretical solution that separates the mechanical and magnetic equations. Taking into consideration the inherent coupled behavior of the magnetostrictive material, the stress induced by the magnetic field on the nanocomposite is estimated by accounting for the Lorentz force (f) acting on each iron particle, with its maximum magnitude given by:

$$f = |I_e L \times B(z)| \tag{9}$$

Considering an individual iron particle as a spherical current carrying element, I_e in the above equation is obtained as

$$I_e = M(z)(\pi d) \tag{10}$$

By re-arranging Eq. (9) to substitute expressions for $B(z)$ and I_e, the maximum Lorentz force acting on each particle is obtained as:

$$f = \mu_0 \chi_{particle} (\pi d)^2 H^2 \left(1 - \frac{2z}{t}\Delta\right)^2 \left(1 + \chi_{particle}\right). \tag{11}$$

According to section 3.1, it is assumed that magnetic intensity linearly reduces by penetrating through the composite thickness, resulting in changing the Lorentz force acting on a particle, through the thickness. Therefore, to investigate the total force applied through the thickness (z direction), uniform arrangement of particles in polymer is proposed in this research to find out the approximate numbers of particles and distance between two adjacent particles in the z direction. For this purpose, the composite is divided to several identical sub-cells consisting of a particle and surrounding matrix. The sub-cells have identical volume fractions across the nanocomposite. Thus, if we assume similar number of divisions at each direction (labelled as N_x, N_y, N_z), the dimensions of the sub-cell (d_x, d_y, d_z) will be obtained through the ratio of the number of divisions to the dimensions of the whole composite.

Considering the proposed distribution of the iron particles in the matrix, the total force (f_t) in the z direction is obtained by the accumulation of each individual forces exerted by the particles ($f(n)$):

$$f_t = (NxNy)\sum_{n=1}^{n_z} f(n) \tag{12}$$

Therefore, the total stress at z direction is obtained from:

$$\sigma_z = \frac{f_t}{A} \tag{13}$$

where A is the area of the surface which is exposed to the magnetic field.

Considering Eq. (7), the effective compliance matrix of the composite can be calculated. Therefore, strain-induced in iron-particles embedded polymer subjected to a unidirectional magnetic field is obtained from:

$$\begin{bmatrix} \varepsilon_x \\ \varepsilon_y \\ \varepsilon_z \\ 2\varepsilon_{xy} \\ 2\varepsilon_{yz} \\ 2\varepsilon_{xz} \end{bmatrix} = [S_{eq}] \begin{bmatrix} \sigma_x \\ \sigma_y \\ \sigma_z \\ \sigma_{xy} \\ \sigma_{yz} \\ \sigma_{xz} \end{bmatrix} \tag{14}$$

4. Results and Discussion

The specimens illustrated in Figure 6 were produced as solid blocks, employing the primary printing configurations specified in Table 1. Each category consisted of three printed specimens. By applying a magnetic field comprising two rows (270 mT for every pair of magnets in each row), which were affixed on both sides of the specimens, an approximate deformation of 1.0±0.3 mm in the direction of the magnetic field was induced (the initial boundaries of the cube are indicated by the dashed line, illustrating the printed edges in the absence of a magnetic field). The deformation observed when a three-row magnetic field was employed (300 mT for each set of magnets in each row) amounted to 1.8±0.2 mm.

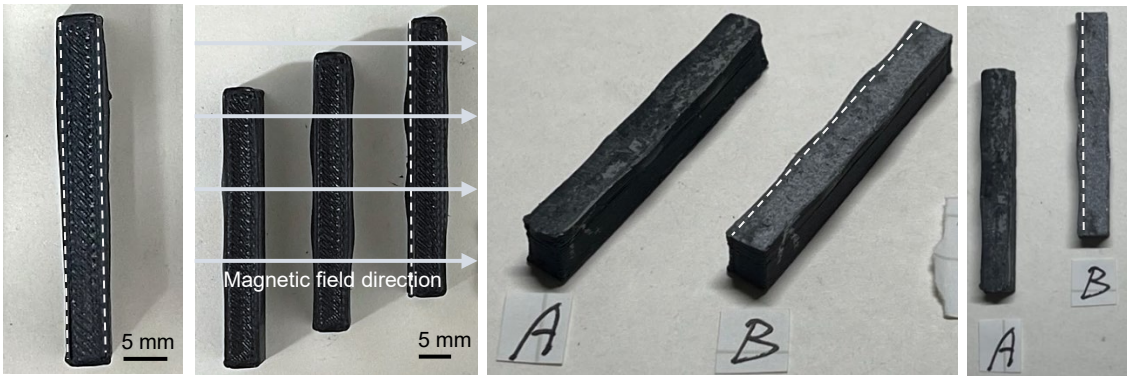

Deformation induced by two-row magnets; Max. 1.0 mm

Deformation induced by three-row magnets Max. deformation 1.8 mm

Figure 6. evolution of deformation induced by magnetic fields during 3D printing with maximum 1.0mm and 1.8mm under two-row and three-row magnets, respectively at 270mT and 300mT

Optical microscopic observations on the printed blocks showed non-uniform distribution and dispersion of the iron particles, with dimensions varied between 5 and 100 microns, shown typically in Figure 7, where the particles are identified as bright spots on grey PLA background.

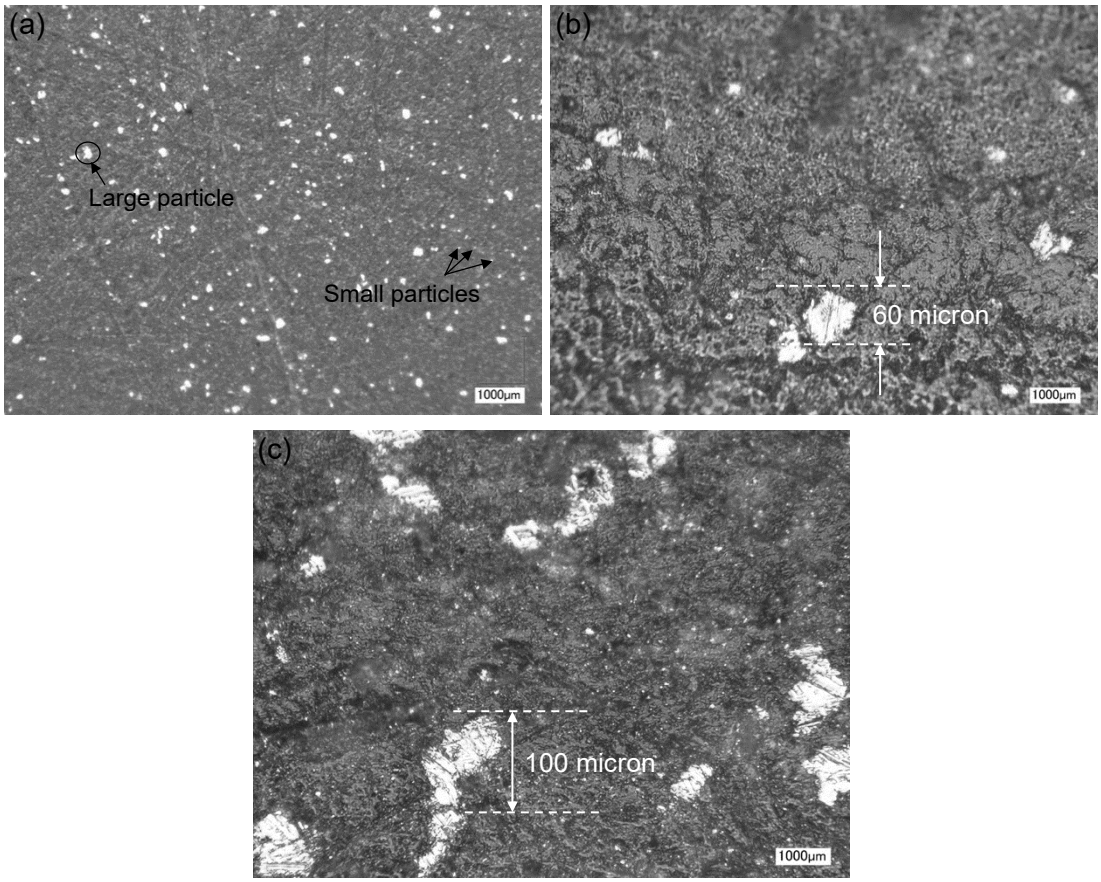

Figure 7: Cut-section view of magnetic nanocomposite

Through optical microscopy of the material after printing, it has been observed that the application of a magnetic field during 3D printing, when the material is heated to approximately 200°C and deposited, causes a noticeable deformation towards the direction of the applied field. This direction appears to be symmetric with respect to the central axis, identified as the dashed line in Figure 8. The observed deformation arises from the movement of magnetised particles within the polymer, which becomes softer at higher temperatures. This movement primarily generates mechanical strains at the interface between the rigid particles and the polymer, aligning them in the direction of the applied magnetic field. These observations were made within the effective field area depicted in Figure 9, where the field's lines of force showed a relatively high level of alignment. Furthermore, it was noted that the ferromagnetic particles closer to the magnets exhibited higher levels of magnetisation (as shown in Section 3), resulting in greater deformation compared to those in the central area, which displayed an approximately neutral magnetic push-pull state. The expressions developed in Section 3 describe the deformation's evolution based on the distance from a magnetised surface within a relatively thick material (our specimens). The subsequent section provides a quantitative analysis of these expressions.

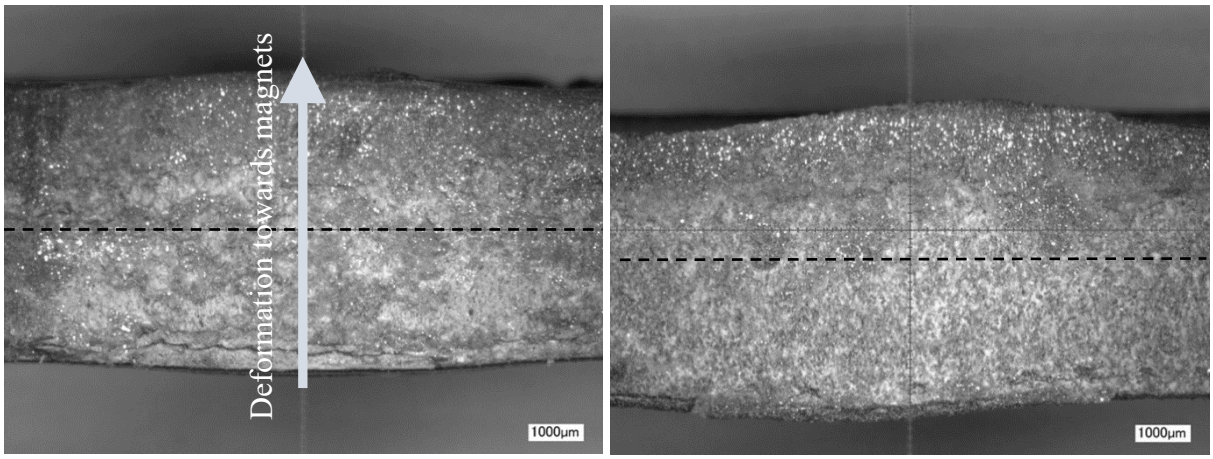

(a) (b)

Figure 8: a) Cut from symmetrically deflected sample, magnification of x30, b) Cut from asymmetrically deflected sample, magnification of x30

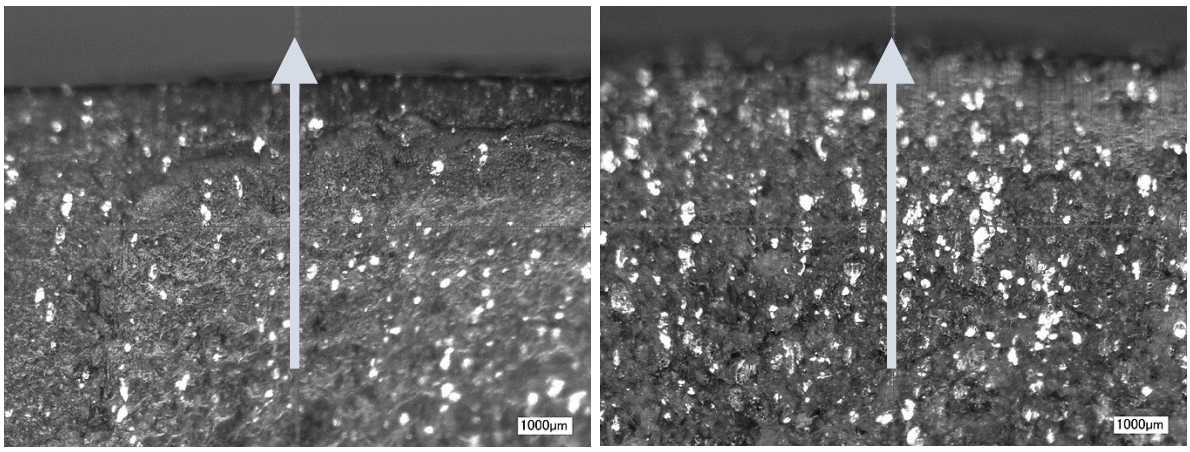

(a) (b)

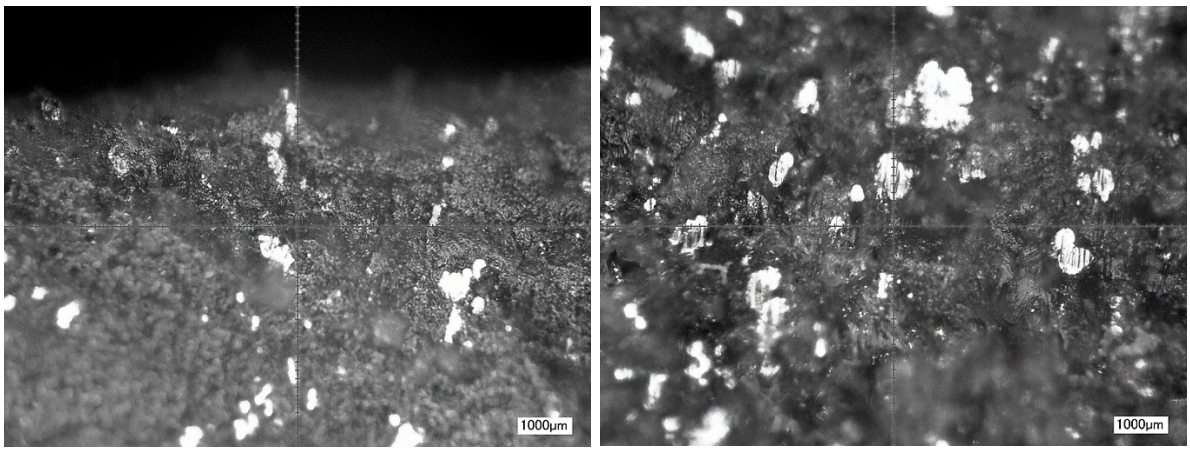

(c) (d)

Figure 9: Magnified views of the cuts shown in Figure 8 with the preferred orientation taken by the particles inside the PLA matrix, as observed post printing in different locations local to the surface close to the magnets (a-d) (arrow showing deformation direction towards the magnets)

Further investigation using 3D reconstruction image processing on the material using IPSDK (supplied by Reactive'IP) showed microparicle size (averaged diameter) ranged from 7 to 100 microns, with the majority of particles (~70%) falling withing 10micron in diameter (Figure 10). The analysis also showed a particle distribution of 10.2 Vol.%. The reconstruction of particles with averaged size of smaller than 5 micron was not conducted as they were rarely present in the polymer matrix.

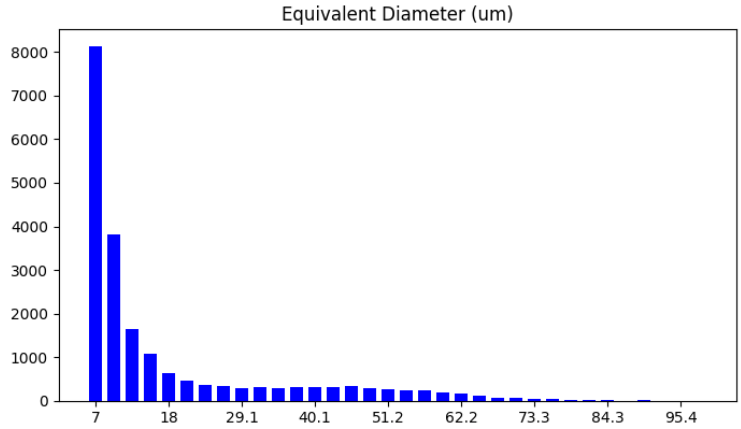

Figure 10. Quantification of size and number distribution of iron microparticles using IPSDK

5. Theoretical solution:

Based on the explanations given earlier, a particle diameter of 10 microns was selected for the theoretical calculations. A gaussmeter, which operates on the principle of the Hall effect, was utilised to detect and measure the strength of the magnetic field. The Hall effect principle depends on the observation that charge carriers in a conductor can have positive or negative charges, and the density of these carriers per unit volume of the conductor can be determined. [30]. A voltmeter was connected across the width of the strip to measure the potential difference between its two edges. The voltmeter also indicated which edge had a greater potential. Using this approach, the equilibrium between electric and magnetic forces was determined. To be precise, an SDL900 DC Extech gaussmeter (product EXTESDL90) was employed to gauge the magnetic field strength in mT through the utilisation of the Hall effect (Figure 11). This was conducted in conjunction with a field pattern visualizer film.

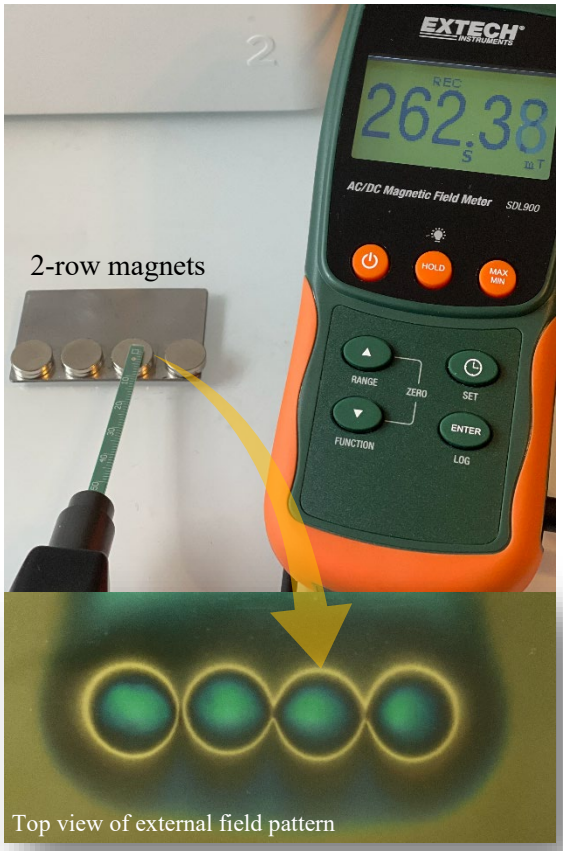

Figure 11. Magnetic field measurement of the magnets setup on a steel strip using Extech gaussmeter, (a) displaying a field strength of 262.4 mT and S-pole for two-row magnets,

It is essential to note that the size distribution of magnetic reinforcements within the polymer after 3D printing varied from nanometers to tens of microns. The largest particles reached a diameter of nearly 100 microns though in few numbers observed. The value of Δ, which signifies the reduction percentage of the magnetic field at the central axis of the nanocomposite (at half the thickness), has been measured empirically.

The material properties utilized in the theoretical calculations were displayed in Tables 2 and 3, respectively.

Table 2. Mechanical properties of the iron particles

Parameter	Value
E (Gpa)	211
ν	0.29

The temperature significantly affects the elastic modulus of PLA, as demonstrated in Figure 12 [31]. Considering the high temperatures involved in the 3D printing process, it is crucial to take into account the temperature's impact on PLA properties. In this study, the temperature was initially assumed to be the average value between the nozzle and bed temperatures, approximately 130°C. However, the actual temperature during the deposition may have been higher and closer to the nozzle temperature. Figure 12 shows that a mere 5°C difference beyond the 160°C threshold results in a drastic 45-fold reduction in the modulus. For instance, at 170°C compared to 165°C (indicated by arrows in the figure). We have also incorporated these reductions into our theoretical calculations.

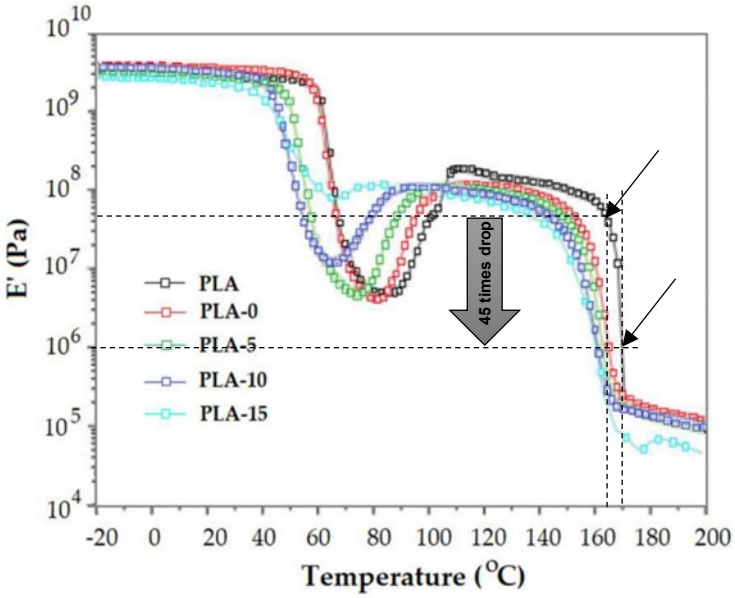

Figure 12. Temperature dependence of the elastic modulus for neat PLA and PLAs plasticized with dioctyl phthalate (DOP) [31]

Table 3. Mechanical properties of the PLA at 130°c

Parameter	Value
E (Mpa)	100
ν	0.33

For the theoretical calculation of magnetic field-induced deformation, we assume that all iron particles are spherical with a diameter of 10 microns. Moreover, the magnetic field at the effective length of the sample and the reduction percentage (Δ) were measured to be approximately 260 mT and 80%, respectively. Based on these measurements, we obtained results for the magnetic field-induced stress, strain, and deformation in the z-direction using the equations outlined in Section 3. These results are compiled and presented in Table 4. The field value is highly sensitive to the distance from the magnets. Although the field at the magnet's surface is 260 mT, it can decrease to 60-70 mT within a few millimeters distance and on the sample's surface, as observed in our measurements. We have taken this into account in our calculations. The strains developed due to such a reduction in the field (to 65 mT) are 10 times smaller than those at 260 mT as calculated in Table 4.

Table 4. Theoretical solution

Parameter	Value
σ_z(Mpa)	18.50
ε_z	0.11
u_z (mm)	< 0.27

When moving from the surface exposed to the magnetic field towards the central axis, the magnitude of strain decreases on the local surfaces. This behaviour can be attributed to the reduction of the magnetic field intensity, which occurs as the magnetic field lines spread out and disperse with increasing distance from the magnets.

Upon comparing the analytical and experimental results, an apparent disparity is observed between the outcomes. This difference can mainly be attributed to the uncertainty surrounding the temperature of the PLA material throughout the 3D printing process. As the composite filament is extruded from the nozzle and makes contact with the cooler bed, it rapidly loses heat and solidifies within a few seconds. The precise temperature at which solidification occurs can be challenging to measure accurately due to several factors, including ambient temperature, print speed, and layer thickness. Additionally, in the proposed model, the magnetic field was applied to the printed sample simultaneously with the printing process, further complicating the temperature measurement.

As mentioned earlier, the temperature was assumed to be 130°C. However, it is highly probable that the actual temperature exceeded this value, particularly in the upper layers which are exposed to the magnetic field. According to Figure 11, the Young's modulus of PLA is approximately 100 MPa at 130°C. However, beyond 160°C, the modulus drops significantly, reaching approximately 45 MPa at 165°C and 1 MPa at 170°C. This demonstrates an ultra-high sensitivity of mechanical properties to small variations of temperatures, and hence field-induced deformation. These lower elastic modulus values result in larger magnetic field-induced deformations, as shown in Table 5. At approximately 170°C, i.e., a closer value to the nozzle temperature, a theoretical deformation value of 1.3 mm is obtained from the theoretical expressions developed in section 3, in agreement with that observed in the 3D printed part.

Table 5. Magnetic field-induced deformations of iron/epoxy composite at two deferent temperatures

Temperature (°C)	PLA Young Modulus (MPa)	Field induced deformation (mm)
165	45.0	0.04
170	1.0 (45 times smaller than above)	1.30 (33 times larger than above)

It is evident from the table above that accurately quantifying the temperature of PLA has a significant impact on our results. Therefore, it is crucial to develop a method for precisely measuring the temperature of each layer during the 3D printing process. Additionally, there are several other factors that contribute to the accuracy of the theoretical expression developed in this research, including:

- The assumption of spherical iron particles with uniform dimensions is not entirely valid. During the multi-material mixing, extrusion, and 3D printing process, the particles can vary in size and shape, resulting in a non-uniform size distribution.
- Further investigation is needed to validate the assumption of a linear reduction in the magnetic field as it penetrates through the thickness.
- The magnetic behaviour in magnetostrictive materials is coupled with temperature. Since the experiment is conducted at high temperatures, the level of magnetisation can be affected.
- Solving a boundary value problem considering a coupled magneto-thermo-viscoelastic constitutive model and boundary conditions of the structure is necessary to accurately determine strain, stress, and magnetic fields in the structure.
- When iron particles are magnetised, they generate internal magnetic fields that exert forces on the surrounding particles. However, this aspect has not been investigated in the theoretical derivation. Such phenomena would produce an accumulative

magnetisation effect on the actual induced strains. Assuming that the field is uniform in a 2D particle matrix element containing a few particles located at distance z from a magnetized surface, the Faraday's law of electromagnetic induction can be applied to calculate the electric field generated inside one particle due to the magnetic field of the neighboring particle (e.g., $\nabla \times E_1 = -dB_2/dt$, where 1 and 2 are the neighboring particles). Similarly, $\nabla \times E_2 = -dB_1/dt$. Although the influence of E_1 and E_2 on the force and strain between the particles is unclear, the force typically depends on B_1, B_2, and the distance between them (d). Therefore, the mechanical stress-strain field induced inside the polymer at a distance from a particle can be calculated by accounting for such interactive fields. This observation also highlights the fact that, despite a unidirectional field application through the thickness (in the z direction), a triaxial strain field can be induced between the particles, as illustrated as ε_{local} in Figure 13. In such cases, the morphological features associated with the particle distribution and dispersion are expected to significantly affect the accurate estimation of ε_{local}. The authors are currently investigating this aspect by implementing a multiphysics finite element analysis approach.

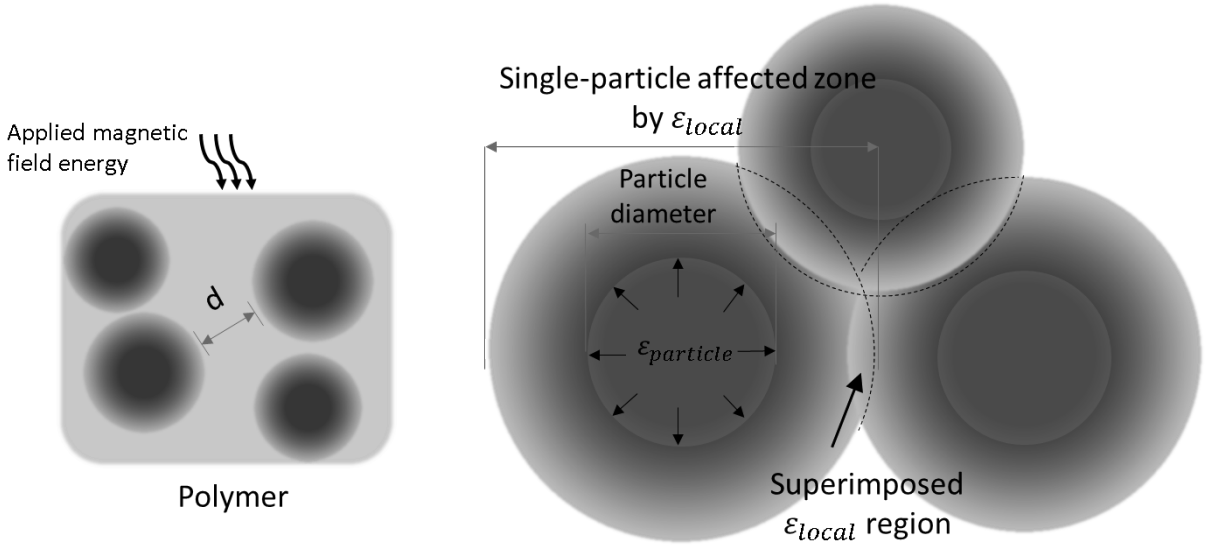

Figure 13. Schematic illustration of interactive, accumulative strain field induced by the magnetisation of neighbouring particles

These additional factors need to be thoroughly examined to gain a comprehensive understanding of the observed differences.

6. Conclusions

Permanent deformation was observed during the 3D printing of PLA polymers embedded with iron particles, which were subjected to a constant magnetic field *in situ*. This was achieved by utilising relatively low magnetic fields generated by fixing circular Neodymium magnets in the vicinity of the region where the nanocomposite was being printed. The observed deformation occurred predominantly in the direction of the theoretical magnetic force lines, that is, towards the position of the magnets. It symmetrical developed on both sides of the nanocomposite sample. The primary opportunity created by these observations is the utilisation of the magnetic field to tailor the direction and variable geometry during a 3D printing or magnetic polymer composite manufacturing process.

A simplified theoretical constitutive equation has been developed to describe the extrinsic strains and average deformation induced by a magnetic field. This equation considers linear

Multiphysics phenomena that occur through the mechanical and magnetic response of the nanocomposite. It has been observed that the simplified decoupled theory proposed in this paper accurately describes the strains experienced during the 3D printing process, provided that precise temperature values for the layers are provided during printing. The theory also predicts a highly sensitive field-induced deformation in response to temperature variations. Further investigations are required to expand the proposed theory to include nonlinear Multiphysics phenomena, as explained in section 5, and to incorporate temperature variables and coupling effects. Additionally, real-time sensing of strains, temperature, and magnetic induction at different locations (i.e., thicknesses) in the composite during the printing process should be incorporated through further instrumentation.
In general, tailoring the geometry through magnetic-assisted 3D printing holds potential for future magnetic tooling in composite manufacturing and the development of related technologies. However, it is important to consider the uncertainties associated with the strong dependence of thermomechanical properties on layer temperature and the decay of magnetic fields in the future design of magnetic field-assisted composite manufacturing.

Acknowledgments
The authors are grateful of the funding received by the UK Engineering and Physical Sciences Research Council for a Doctoral Training Programme (Grant Ref. EP/W524608/1). The authors would also like to thank Tristan Lowe at the Henry Moseley X-ray Imaging Facility, Photon Science Institute, Alan Turing Building and Henry Royce Institute for micro-computed tomography measurements, and Joseph Baptista for evaluations of particles size and distribution via IPSDK. The underpinning data can be accessed at DOI: 10.25383/city.22960547

References

1. Pearson, C., et al., *Magnetic field assisted 3D printing of short carbon fibre-reinforced polymer composites.* Materials Today: Proceedings, 2022. **64**: p. 1403-1411.
2. Joralmon, D., et al., *Magnetic field assisted 3D printing of limpet teeth inspired polymer matrix composite with compression reinforcement.* Manufacturing Science and Engineering, 2021. **144**(4): p. 1-45.
3. Daminabo, S.C., et al., *Fused deposition modeling-based additive manufacturing (3D printing): techniques for polymer material systems.* Materials Today Chemistry, 2020. **16**: p. 100248.
4. H, Y.N., et al. *Impact damage response of carbon fibre-reinforced aerospace composite panels*. 2015.
5. Croft, K., et al., *Experimental study of the effect of automated fiber placement induced defects on performance of composite laminates.* Composites Part a-Applied Science and Manufacturing, 2011. **42**(5): p. 484-491.
6. Kechagias, J. and D. Chaidas, *Fused filament fabrication parameter adjustments for sustainable 3D printing.* Materials and Manufacturing Processes, 2023. **38**(8): p. 933-940.
7. An, D., et al., *Strain Self-Sensing Tailoring in Functionalised Carbon Nanotubes/Epoxy Nanocomposites in Response to Electrical Resistance Change Measurement.* 9th International Conference on Through-life Engineering Services, 2020.
8. D, L., et al. *Development of damage tolerant composite laminates using ultra-thin interlaminar electrospun thermoplastic nanofibres*. 2018.
9. An, D., et al., *Ultra-thin electrospun nanofibers for development of damage-tolerant composite laminates.* Materials Today Chemistry, 2019. **14**: p. 100202.

10. Henderson, L., et al., *Altering magnetic properties of iron filament PLA using magnetic field assisted additive manufacturing (MFAAM).* Journal of Magnetism and Magnetic Materials, 2021. **538**: p. 168320.
11. Li, D., et al., *Electromagnetic field controlled domain wall displacement for induced strain tailoring in BaTiO3-epoxy nanocomposite.* Scientific Reports, 2022. **12**(1): p. 7504.
12. Calascione, T.M., et al., *Controlling magnetic properties of 3D-printed magnetic elastomer structures via fused deposition modeling.* AIP Advances, 2021. **11**(2): p. 025223.
13. Amirov, A., et al. *3D Printing of PLA/Magnetic Ferrite Composites: Effect of Filler Particles on Magnetic Properties of Filament*. Processes, 2022. **10**, DOI: 10.3390/pr10112412.
14. Yu, B., et al., *Preparation and properties of poly (lactic acid)/magnetic Fe3O4 composites and nonwovens.* RSC Advances, 2017. **7**: p. 41929.
15. Moradi, M., et al., *Simultaneous FDM 4D printing and magnetizing of iron-filled polylactic acid polymers.* Journal of Magnetism and Magnetic Materials, 2023. **568**: p. 170425.
16. CO, M., et al., *Accelerated microwave curing of fibre-reinforced thermoset polymer composites for structural applications: A review of scientific challenges.* Composites Part A: Applied Science and Manufacturing.
17. Avancini, T.G., et al., *Magnetic properties of magnetite-based nano-glass-ceramics obtained from a Fe-rich scale and borosilicate glass wastes.* Ceramics International, 2019. **45**(4): p. 4360-4367.
18. Yi, S., et al., *High-throughput fabrication of soft magneto-origami machines.* Nature Communications, 2022. **13**(1): p. 4177.
19. Wang, B., et al., *The influence of particle chain-magnetic field spatial location, frequency, dynamic strain amplitude and the prestrain on the mechanical performance of anisotropic magneto-rheological elastomer.* Polymer Testing, 2021. **104**: p. 107411.
20. Lucarini, S., M. Hossain, and D. Garcia-Gonzalez, *Recent advances in hard-magnetic soft composites: Synthesis, characterisation, computational modelling, and applications.* Composite Structures, 2022. **279**: p. 114800.
21. Alapan, Y., et al., *Reprogrammable shape morphing of magnetic soft machines.* Science Advances. **6**(38): p. eabc6414.
22. Hu, X., et al., *Multifunctional thermo-magnetically actuated hybrid soft millirobot based on 4D printing.* Composites Part B: Engineering, 2022. **228**: p. 109451.
23. Yarali, E., et al., *Magneto-/ electro-responsive polymers toward manufacturing, characterization, and biomedical/ soft robotic applications.* Applied Materials Today, 2022. **26**: p. 101306.
24. Kadapa, C. and M. Hossain, *A unified numerical approach for soft to hard magneto-viscoelastically coupled polymers.* Mechanics of Materials, 2022. **166**: p. 104207.
25. Filipcsei, G., et al., *Magnetic Field-Responsive Smart Polymer Composites*, in *Oligomers - Polymer Composites - Molecular Imprinting*, B. Gong, A.R. Sanford, and J.S. Ferguson, Editors. 2007, Springer Berlin Heidelberg: Berlin, Heidelberg. p. 137-189.
26. Ponomarenko, A.T., et al., *Magnetic-field-sensitive polymer composite materials.* Smart Materials and Structures, 1994. **3**(4): p. 409.
27. Ryu, S., et al., *Micromechanics-based homogenization of the effective physical properties of composites with an anisotropic matrix and interfacial imperfections.* Frontiers in Materials, 2019. **6**.

28. Lee, S., et al., *Applicability of the interface spring model for micromechanical analyses with interfacial imperfections to predict the modified exterior Eshelby tensor and effective modulus.* Mathematics and Mechanics of Solids, 2019. **24**.
29. Zhan, Y.-S. and C.-h. Lin, *Micromechanics-based constitutive modeling of magnetostrictive 1–3 and 0–3 composites.* Composite Structures, 2021. **260**: p. 113264.
30. Halliday, D., R. Resnick, and J. Walker, *"Principles of Physics"*. 9th ed.
31. Cristea, M., D. Ionita, and M.M. Iftime *Dynamic Mechanical Analysis Investigations of PLA-Based Renewable Materials: How Are They Useful?* Materials, 2020. **13**, DOI: 10.3390/ma13225302.